



(RESEARCH ARTICLE)



## Molecular docking study of seventy-six phytomolecules from sixteen aromatics medicinal plants as promising inhibitors of five non-structural proteins of SARS-CoV-2

Tendrinarisoa RANDRIAMAMISOLONIRINA <sup>1,\*</sup> and Fridolin Olivier MAMINIAINA <sup>1,2,3</sup>

<sup>1</sup> Malagasy Institute of Veterinary Vaccines (IMVAVET), Ministry of Higher Education and Scientific Research, BP 04 Rue Farafaty Ampandrianomby Antananarivo Madagascar.

<sup>2</sup> FOFIFA-Department of Zootechnical, Veterinary and Fish Research (FOFIFA-DRZVP), Ministry of Higher Education and Scientific Research, BP 04 Rue Farafaty Ampandrianomby Antananarivo Madagascar.

<sup>3</sup> Department of Veterinary Science and Medicine, Faculty of Medicine, Ministry of Higher Education and Scientific Research, BP 04 Rue Farafaty Ampandrianomby Antananarivo Madagascar.

GSC Biological and Pharmaceutical Sciences, 2022, 20(03), 227–250

Publication history: Received on 01 August 2022; revised on 12 September 2022; accepted on 14 September 2022

Article DOI: <https://doi.org/10.30574/gscbps.2022.20.3.0345>

### Abstract

Since the identification of COVID-19 in China in December 2019, scientists and researchers have been continuously discovering and proposing drugs for this disease. Many efforts have been made to examine medicinal plants known for their benefits in treating infectious diseases and for their actions in boosting of the immune system. Repurposing of FDA-approved antiviral drugs has also been advanced. However, no effective antiviral drug specific to COVID-19 is currently available. To contribute in the search for drugs against this disease, the present study aims to identify secondary metabolites (or phytomolecules) possessing an inhibitory effect on the replication of SARS-CoV-2, the etiological agent of COVID-19.

76 secondary metabolites from 16 aromatics medicinal plants from Madagascar were uploaded to the PubChem server. Then, they were docked with 5 non-structural proteins (nsps) of SARS-CoV-2, including the main protease, the papain-type protease, the RNA-dependent RNA polymerase, the helicase and the 2'-O-methyltransferase, using the Autodock Vina program integrated in the PYRIX 0.8 software.

The results show that 5 secondary metabolites of *Cinnamosma fragrans* (Capsicodendrin, Ugandensolide, Cinnamolide, Tocotrienol and Pereniporin B) have good affinity with the 5 nsps of SARS-CoV-2 and can inhibit its functions in viral replication. Therefore, these phytomolecules could be used in the development of antiviral drugs against SARS-CoV-2 and COVID-19. Nevertheless, further *in vitro* and *in vivo* studies should be performed to valorize these results obtained by the *in silico* method.

**Keywords:** COVID-19; SARS-CoV-2; Non-structural protein; Secondary metabolites; Aromatics medicinal plants; Molecular docking

### 1. Introduction

At the end of 2019, a new disease named COVID-19 and caused by a new coronavirus, known as Severe Acute Respiratory Syndrome Coronavirus-2 or SARS-CoV-2 has been reported in China [1]. This disease has quickly spread throughout the world and is now causing a global pandemic worldwide. In December 2021, more than 9.49 million deaths have been reported worldwide [2]. However, this number has continued to increase due to the emergence of

\*Corresponding author: Tendrinarisoa RANDRIAMAMISOLONIRINA

Malagasy Institute of Veterinary Vaccines (IMVAVET), Ministry of Higher Education and Scientific Research, BP 04 Rue Farafaty Ampandrianomby Antananarivo Madagascar.

new variants of SARS-CoV-2 such as Omicron [3]. Faced with this situation, many pharmaceutical companies are trying to develop vaccines or drugs that will control the situation. Unfortunately, no pharmaceutical product has been approved as safe, effective and specific for the treatment and prevention of COVID-19. Only precautionary measures such as border surveillance, practicing self-hygiene, social distancing and wearing personal protective equipment are being practiced to prevent the spread of the disease.

In Madagascar and in other countries of the world, most of peoples have also used medicinal plants such as *Artemisia annua*, *Eucalyptus globulus*, *Allium sativum*, *Zingiber officinalis* and many others to fortify the medicines offered by the doctors [4-6]. Although the pharmacological importance of these plants in other infectious diseases is well documented, no conclusive experimental results have been found to prove their effectiveness in the treatment of COVID-19.

Currently, advances in bioinformatics have made it possible to screen bioactive compounds in plants and to evaluate their pharmacological properties [7]. In order to contribute to the search for drugs against COVID-19, this study aims to identify phytomolecules with an inhibitory effect on SARS-CoV-2 replication in sixteen aromatic medicinal plants from Madagascar. The results of these studies can be used in other *in vitro* and/or *in vivo* studies to develop an effective drug against this disease.

## 2. Material and methods

### 2.1. Selection and preparation of ligands

In this study, we selected seventy-six secondary metabolites (phytomolecules) from six-teen aromatic medicinal plants from Madagascar. The information about these phytomolecules and their percentages in the selected plants are summarized in Supplementary Table 1. The structure data file (.*sdf*) in two-dimensional (2D) or three-dimensional (3D) formats and the canonical SMILES files of these 76 selected phytomolecules were downloaded to the PubChem database ([www.pubchem.ncbi.nlm.nih.gov](http://www.pubchem.ncbi.nlm.nih.gov)). They are used in molecular docking studies.

### 2.2. Selection and preparation of receptors

We selected five non-structural proteins (nsps) from SARS-CoV-2, including main protease (Mpro), papain-like protease (PLpro), RNA-dependent RNA polymerase (RdRp), helicase and 2'-O-methyltransferase (2'-O-Mtase). These proteins are selected for their involvement in virus replication and in the host immune response [8, 9].

Their 3D structures were retrieved from the RCSB PDB database (<http://www.rcsb.org>), using the identification numbers shown in Table 1. Then, the co-crystallized ligands and water molecules in those structures were removed, using Discovery Studio Visualizer version 2017 or D.S v2017 software (<http://accelrys.com/products/collaborative-science/biovia-discovery>) [10]. Afterwards, the structures without ligands were minimized in the UCSF CHIMERA software, using the Amber force field ff94 [11]. Finally, the minimized structures are saved in .*pdb* format in the same software.

**Table 1** The non-structural proteins used in this study

Protein	PDB ID	Organism	Expression System	Resolution	Method	Chain	Author of deposition
Nsp5 (Mpro)	6LU7	SARS-CoV-2	<i>Escherichia coli</i> BL21(DE3)	2,16 Å	X-ray diffraction	A	[12]
Nsp3 (PLpro)	6WUU	SARS-CoV-2	<i>Escherichia coli</i> BL21(DE3)	2,79 Å	X-ray diffraction	A	[13]
Nsp12 (RdRp)	6M71	SARS-CoV-2	<i>Escherichia coli</i> BL21(DE3)	2.90 Å	Electron microscopy	A	[14]
Nsp13 (Helicase)	6ZSL	SARS-CoV-2	<i>Escherichia coli</i>	1,94 Å	X-ray diffraction	B	[15]
Nsp16 (2'-O-Mtase)	6YZ1	SARS-CoV-2	<i>Escherichia coli</i> BL21(DE3)	2,40 Å	X-ray diffraction	A	[16]

### 2.3. Determination of receptor active site residues

The amino acid (aa) residues composing the active site of the targeted nsps were predicted using COACH-D server (<http://yanglab.nankai.edu.cn/COACH-D/>). This server is the improved version of the COACH server and uses five individual methods to predict protein-ligand binding sites [17]. In the prediction, we submitted in the server the previously prepared 3D structures of nsps. Then, computations were performed by the server and the best predicted results were proposed. Among the proposed results, we selected only the residues appearing in the first rank (whose confidence scores are also high). The positions of these residues in the 3D structure of the nsps are visualized using the D.S v2017 software.

### 2.4. Molecular docking

Molecular docking was performed using the PYRX 0.8 software (<http://pyrx.sourceforge.net/downloads>) [18]. Before docking, the 3D structures of the receptors (nsps) were imported into the PYRX 0.8 software in .pdb format. Then, the 3D structures of the ligands (phytomolecules) were uploaded in .sdf format and were minimized using Open Babel, a tool integrated in the same software [19]. Afterwards, the receptor and ligand files were converted to .pdbqt formats via the Autodock4 [20]. During docking, all ligands are considered as flexible and all receptors are considered as rigid. The grid box parameters are configured using the X, Y, Z coordinates summarized in Table 2. All docking calculations are performed with the program AutoDock Vina [21]. After docking, the complexes with the lowest binding energy (kcal/mol) were selected and the interaction modes of phytomolecules with nsps are visualized in D.S v2017.

**Table 2** X, Y, Z coordinates of the grid box

Proteins	Center coordinates			Size coordinates		
	X	Y	Z	X	Y	Z
Mpro	-12.8126	13.6373	69.0252	19.9863	25.8721	27.6913
PLpro	22.9610	66.1449	6.3847	29.0950	28.5568	29.6469
RdRp	110.7355	105.5276	123.7700	33.6206	47.3115	25.5036
Helicase	-30.3493	35.3954	-30.3493	42.1182	37.8497	35.7217
2'-O-MTase	83.4814	15.2410	28.0836	19.1923	23.2438	22.6208

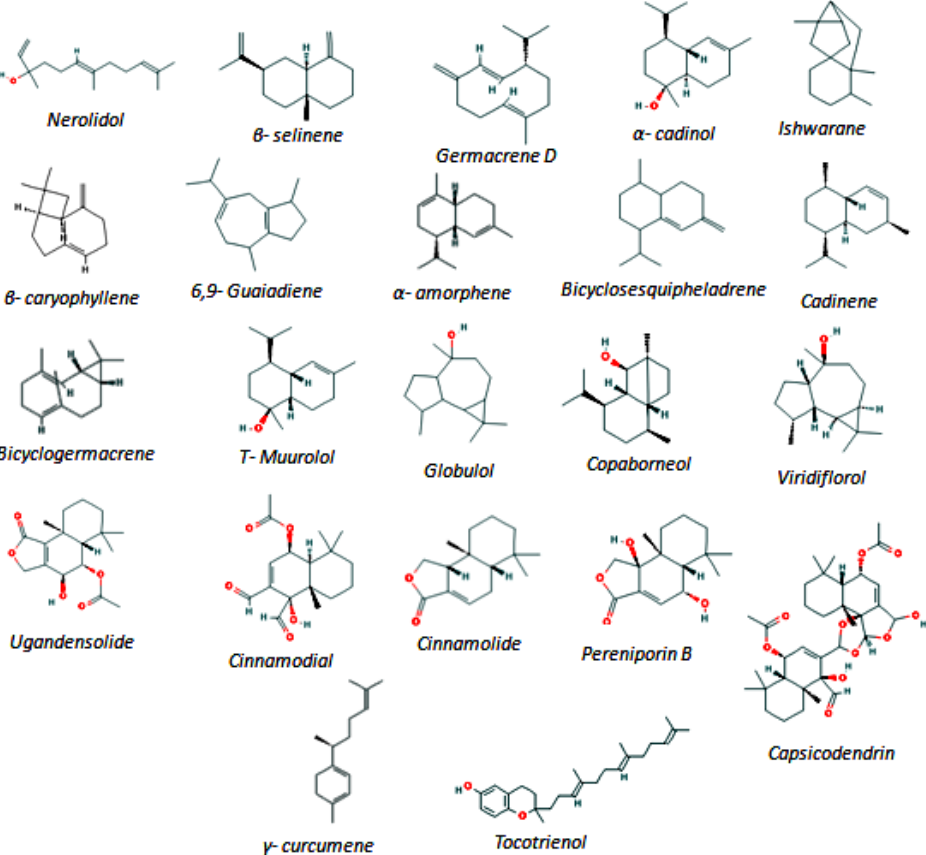
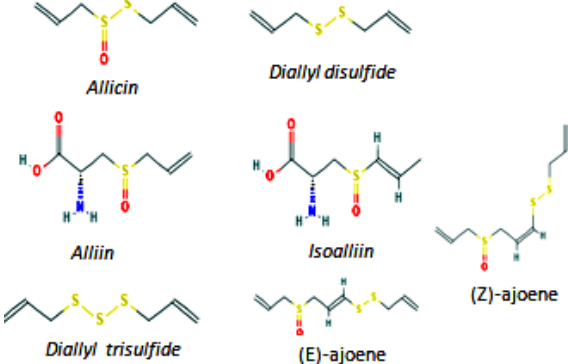
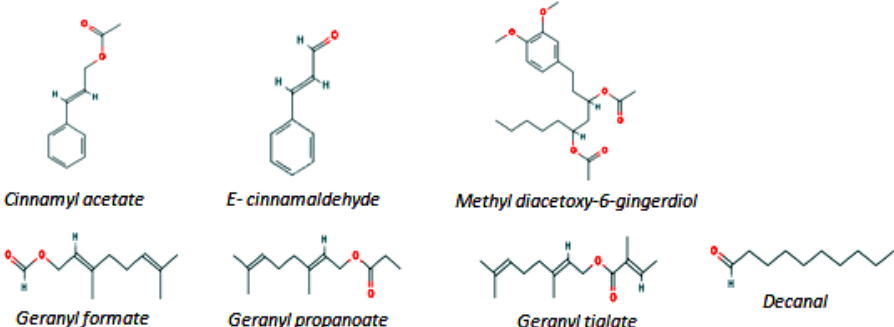
## 3. Results

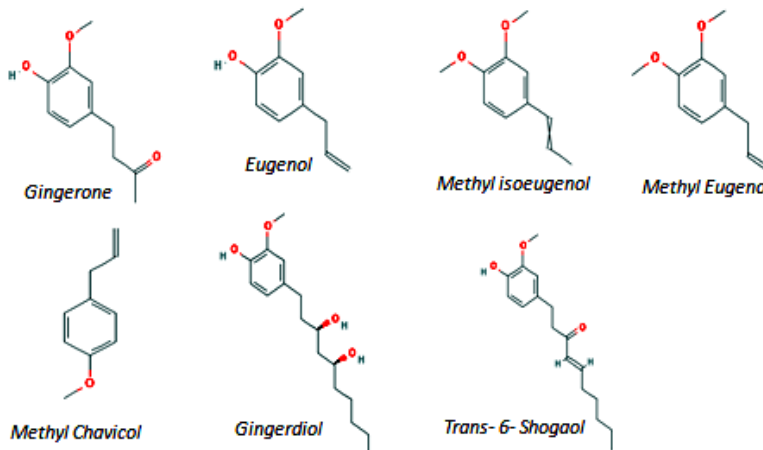
### 3.1. Selected ligands

Among the seventy-six phytomolecules selected, fifty-five phytomolecules are classed in the terpenoid family. They include thirty-three monoterpenes and twenty-two sesquiterpenes (Table 3). The remaining twenty-one phytomolecules are organo-sulfur, organo-oxygen and aromatic compounds. These results indicate that most of the selected phytomolecules are terpenoids.

**Table 3** Classification and 2D structures of the 76 phytomolecules used in this study

Classification of Phytomolecules	Numbers	Names and 2D structure of ligands
Monoterpenes	33	

Sesquiterpenes	22	 <p> <i>Nerolidol</i>, <i>β-selinene</i>, <i>Germacrene D</i>, <i>α-cadinol</i>, <i>Ishwarane</i>,  <i>β-caryophyllene</i>, <i>6,9-Guaiadiene</i>, <i>α-amorphene</i>, <i>Bicyclosesquipheladrene</i>, <i>Cadinene</i>,  <i>Bicylogermacrene</i>, <i>T-Muurolol</i>, <i>Globulol</i>, <i>Copaborneol</i>, <i>Viridiflorol</i>,  <i>Ugandensolide</i>, <i>Cinnamodial</i>, <i>Cinnamolide</i>, <i>Pereniporin B</i>, <i>Capsicodendrin</i>,  <i>γ-curcumene</i>, <i>Tocotrienol</i> </p>
Organo-Sulfur Compounds	7	 <p> <i>Allicin</i>, <i>Diallyl disulfide</i>, <i>Alliin</i>, <i>Isoalliin</i>, <i>(Z)-ajoene</i>,  <i>Diallyl trisulfide</i>, <i>(E)-ajoene</i> </p>
Organo-Oxygenated Compounds	7	 <p> <i>Cinnamyl acetate</i>, <i>E-cinnamaldehyde</i>, <i>Methyl diacetoxy-6-gingerdiol</i>,  <i>Geranyl formate</i>, <i>Geranyl propanoate</i>, <i>Geranyl tiglate</i>, <i>Decanal</i> </p>

Aromatic compounds	7	 <p>Chemical structures of seven aromatic compounds are shown:</p> <ul style="list-style-type: none"> <li>Gingerone</li> <li>Eugenol</li> <li>Methyl isoeugenol</li> <li>Methyl Eugenol</li> <li>Methyl Chavicol</li> <li>Gingerdiol</li> <li>Trans-6-Shogaol</li> </ul>
--------------------	---	--

### 3.2. Target proteins and active site residues

In this study, we targeted five nsps of SARS-CoV-2 including Mpro, PLpro, RdRp, Helicase and 2'-O-MTase. Their 3D structures are retrieved from the RCSB PDB database and the amino acid residues that form their active sites are predicted using COACH-D server. The following paragraphs describe the results obtained after the 3D structure analysis and the prediction of the active site residues of these targeted proteins.

#### 3.2.1. Proteases

Mpro is constituted of 306 amino acid residues (aa), which are divided into three domains including DI, DII, DIII and a long loop. The active site of this enzyme is located in the center of the groove formed by the domains DI and DII (Figure 1A). COACH-D server predicted the following residues Thr<sup>25</sup>, His<sup>41</sup>, Met<sup>54</sup>, Phe<sup>140</sup>, Leu<sup>141</sup>, Gln<sup>142</sup>, Gly<sup>143</sup>, Ser<sup>144</sup>, Cys<sup>145</sup>, His<sup>163</sup>, His<sup>164</sup>, Met<sup>165</sup>, Glu<sup>166</sup>, Pro<sup>168</sup>, His<sup>172</sup>, Asp<sup>187</sup>, Arg<sup>188</sup>, Gln<sup>189</sup>, Thr<sup>190</sup>, Ala<sup>191</sup> and Gln<sup>192</sup> as active site residues of this enzyme.

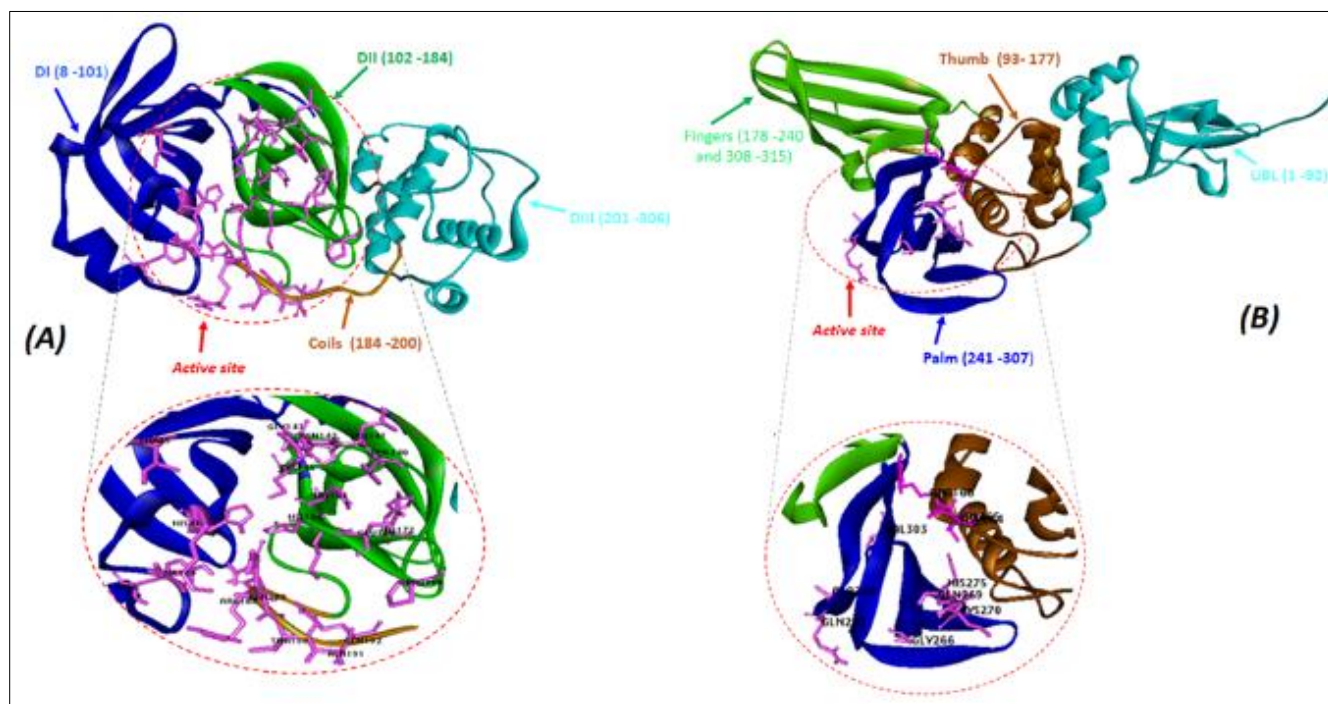


**Figure 1** Structures of the target proteins: (A) main protease or Mpro, (B) papain-like protease or PLpro. The sub-domains that form Mpro and PLpro are shown by different colored ribbons. The active site residues predicted by COACH-D are shown as purple sticks

As for PLpro, it is composed of 316 aa that are divided into five sub-domains: ubiquitin-like (UBL), thumbs, fingers and palm. Its active site is located at the interface of the thumb and palm sub-domains (Figure 1B). The residues Asp<sup>164</sup>, Val<sup>165</sup>, Arg<sup>166</sup>, Ala<sup>249</sup>, Gln<sup>250</sup>, Gly<sup>266</sup>, Gln<sup>269</sup>, Cys<sup>270</sup>, Gly<sup>271</sup>, His<sup>275</sup>, Val<sup>303</sup> were predicted by the COACH-D server as the active site residues of this enzyme. Thus, the three residues forming the triad site Cys<sup>111</sup>, His<sup>272</sup> and Asp<sup>286</sup> of this enzyme were not predicted.

### 3.2.2. RdRp

The RdRp enzyme is composed of 1085aa which is divided into three subunits including nsp12 (chain A, 859aa), nsp7 (chain C, 70aa) and nsp8 (chains B and D, 156aa). Structurally, nsp12 resembles a right hand, comprising the beta hairpins, NIRAN, Interface, finger, palm and thumb sub-domains. The nsp7 and nsp8 subunits bind to the thumb and an additional copy of nsp8 binds to the fingers sub-domain. The active site is located in the palm sub-domain (Figure 2). Upon prediction, COACH-D defined the following residues as active site residues of RdRp: Pro<sup>809</sup>, Glu<sup>811</sup>, Phe<sup>812</sup>, Cys<sup>813</sup>, Ser<sup>814</sup>, His<sup>816</sup>, Thr<sup>817</sup>, Met<sup>818</sup>, Leu<sup>819</sup>, Val<sup>820</sup>, Lys<sup>821</sup>, Gln<sup>822</sup>, Gly<sup>823</sup>, Asp<sup>824</sup>. However, visualization of the positions of these residues at the 3D structure of the enzyme in D.S v2017 excluded the amino acids His<sup>816</sup>, Thr<sup>817</sup>, Met<sup>818</sup>, Leu<sup>819</sup>, Val<sup>820</sup>, Lys<sup>821</sup>, Gln<sup>822</sup>, Gly<sup>823</sup>, Asp<sup>824</sup> among the active site residues (Figure 2).

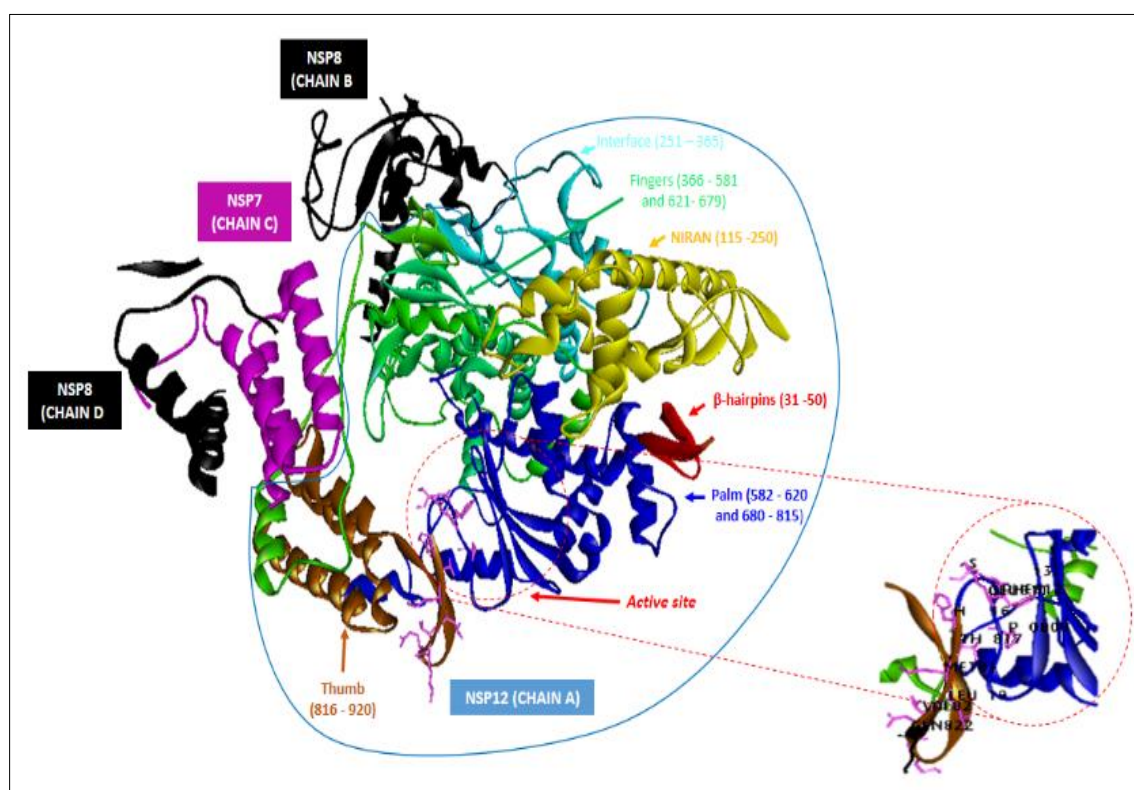


**Figure 2** 3D structures of the RdRp protein of SARS-CoV-2. The different subunits are shown in purple (nsp7), black (nsp8) and circled in blue (nsp12). The different sub-domains of nsp12 are also distinguished:  $\beta$ -hairpins (red), NIRAN (yellow), Interface (light green), Fingers (green), Palm (blue) and thumb (brown). The active site of the enzyme is surrounded by a red line and then expanded

### 3.2.3. Helicase and 2'-O-MTase

The helicase consists of 593aa that correspond to five domains including the N-terminal zinc-binding domain (ZBD), the stalk domain, the 1B domain, the 1A domain, and the 2A domain. The last three domains 1A, 1B, and 2A formed two sites, including the DNA binding site and the ATP hydrolysis site (Figure 3A). Furthermore, prediction of the residues of the helicase active site by the COACH-D server revealed the following amino acids: Leu<sup>256</sup>, Ser<sup>278</sup>, Leu<sup>280</sup>, Gln<sup>281</sup>, Gly<sup>282</sup>, Pro<sup>283</sup>, Pro<sup>284</sup>, Gly<sup>285</sup>, Asp<sup>315</sup>, Thr<sup>367</sup>, Tyr<sup>396</sup>, Pro<sup>434</sup>, Asp<sup>435</sup>, Thr<sup>530</sup>, Thr<sup>532</sup> and Asn<sup>559</sup>. Furthermore, visualization of these amino acids in the 3D structure of the helicase showed that the first thirteen residues were located in the ATP hydrolysis site, whereas the last three residues were located in the DNA binding site (Figure 3A).

The 2'-O-MTase or nsp16 is crystallized with nsp10. This complex is formed by 438aa which is grouped in two chains: the B chain for nsp10 (139aa) and the A chain for nsp16 (299aa). The nsp16 contains a tetrad catalytic site formed by

Lys<sup>46</sup>, Asp<sup>130</sup>, Lys<sup>170</sup> and Glu<sup>203</sup> and two substrate binding pockets including the RNA binding site and the S-adenosylmethionine or SAM binding site (Figure 3B). A total of eighteen amino acids were predicted by COACH-D server to be residues of the 2'-O-MTase active site. A visualization of the position of these residues in the 3D structure of this enzyme via D. S v2017 revealed that the residues Asn<sup>43</sup>, Gly<sup>71</sup>, Ala<sup>72</sup>, Gly<sup>73</sup>, Ser<sup>74</sup>, Ala<sup>79</sup>, Pro<sup>80</sup>, Gly<sup>81</sup>, Asp<sup>99</sup>, Leu<sup>100</sup>, Asn<sup>101</sup>, Gly<sup>113</sup>, Asp<sup>114</sup>, Cys<sup>115</sup>, Asp<sup>130</sup>, Met<sup>131</sup> and Tyr<sup>132</sup> are located in the RNA binding site, whereas Lys<sup>170</sup> is localized in the SAM site (Figure 3B). Indeed, we predicted only the two residues Asp<sup>130</sup>, Lys<sup>170</sup> among the four residues of the tetrad catalytic site Lys<sup>46</sup>-Asp<sup>130</sup>-Lys<sup>170</sup>-Glu<sup>203</sup> of the 2'-O-MTase enzyme.

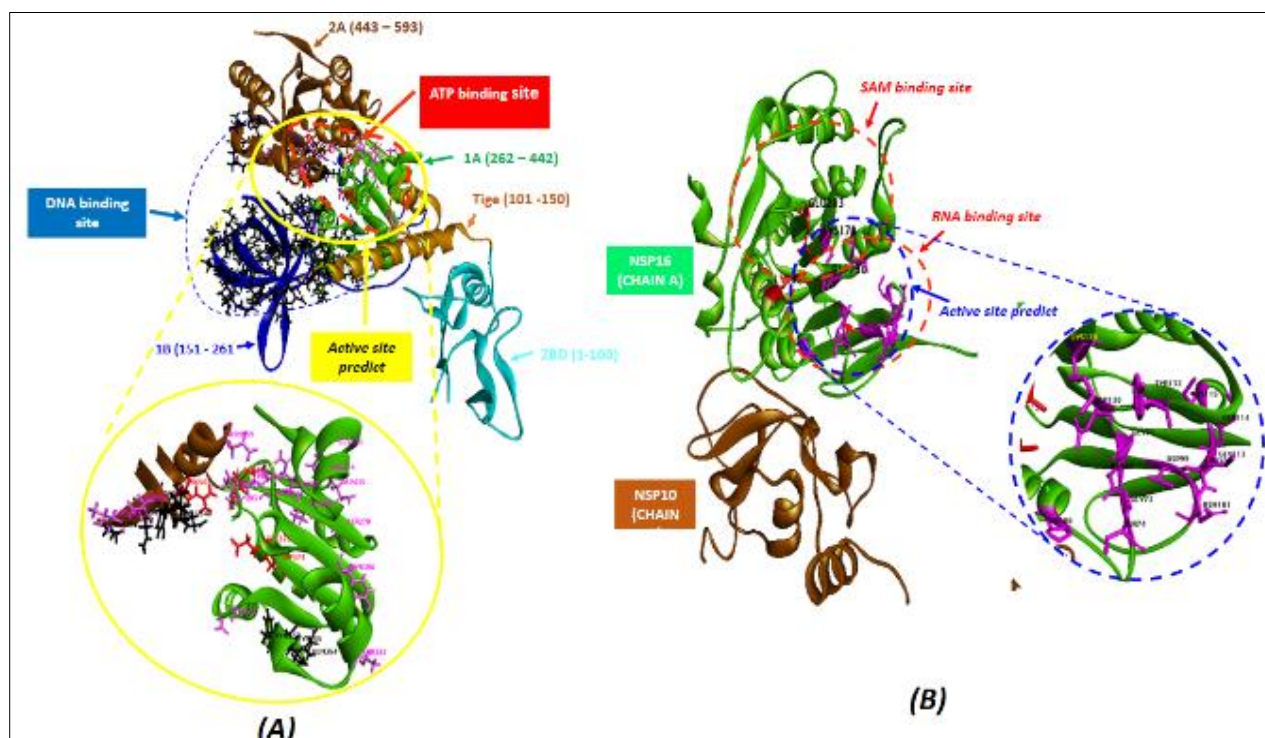


**Figure 3** Structures of helicase and 2'-O-MTase of SARS-CoV-2 : (A) The helicase sub-domains are shown in ribbons of different colors: light green (ZBD), beige (stem), green (sub-domain 1A), Blue (sub-domain 1B) and brown (sub-domain 2A). (B) The different subunits of 2'-O-MTase are also elucidated: nsp10 (brown ribbon) and nsp16 (dark green ribbon)

### 3.3. Molecular docking study

#### 3.3.1. The interaction energies of phytomolecules with target proteins

**Table 4** Molecular docking data represented the 5 phytomolecules with best affinity with 5 SARS-CoV-2 targets

N°	Phytomolecules	Binding energy with target (kcal/mol)				
		Mpro	PLpro	RdRp	Helicase	2'-O-MTase
1	Capsicodendrin	-8.0	-7.3	-7.9	-8.0	-8.1
2	Ugandensolide	-6.4	-6.9	-6.5	-7.8	-6.4
3	Cinnamolide	-6.0	-6.1	-6.3	-6.6	-8.0
4	Tocotrienol	-6.8	-6.4	-6.0	-6.3	-7.2
5	Pereniporin B	-6.0	-6.4	-6.2	-6.9	-6.0

Molecular docking was used to simulate the interactions of the seventy-six selected phytomolecules with the five target nsps. In terms of energy, the results obtained indicated that only five phytomolecules out of the seventy-six tested showed strong interactions with the five target proteins (Table 4). Surprisingly, these five phytomolecules are the



drimane sesquiterpenes of *Cinammosma fragrans*. The others phytomolecules showed lower interaction energies than these five selected phytomolecules (Supplementary table 2).

### 3.3.2. The modes of interaction of phytomolecules with target proteins

The interaction modes of these five selected phytomolecules with Mpro, PLpro, RdRp, Helicase and 2'-O-MTase were visualized in D.S v2017. The following paragraphs summarize the results obtained.

#### Mpro

These five phytomolecules are also well anchored in the active site of Mpro (Figure 4). Indeed, capsicodendrin formed five hydrogen bonds with Thr<sup>26</sup>, Gln<sup>142</sup>, Gly<sup>143</sup>, Ser<sup>144</sup> and Cys<sup>145</sup> and three other hydrophobic bonds with Met<sup>49</sup>, Cys<sup>145</sup> and His<sup>163</sup> (Figure 4A). In addition, Ugandensolide formed two hydrogen bonds with Ser<sup>144</sup> and Cys<sup>145</sup> and two hydrophobic bonds with Cys<sup>145</sup> and His<sup>163</sup> (Figure 4B). In addition, Cinnamolide formed two hydrogen bonds with Leu<sup>141</sup>, Cys<sup>145</sup> and three hydrophobic bonds with Cys<sup>145</sup>/His<sup>163</sup> (Figure 4C). Also, one hydrogen bond with Thr<sup>190</sup> and three hydrophobic bonds with Met<sup>49</sup>, Cys<sup>145</sup> and Met<sup>165</sup> were observed between Tocotrienol and Mpro (Figure 4D). Finally, the interactions of Pereniporin B with Mpro were stabilized only by four hydrogen bonds with Ser<sup>144</sup>, Gly<sup>143</sup> and Cys<sup>145</sup> (Figure 4E). In summary, four phytomolecules (except Tocotrienol) made three or more interactions with the amino acids responsible for protease activity of this enzyme. We suggest that these interactions are sufficient to inhibit the activity of this enzyme.

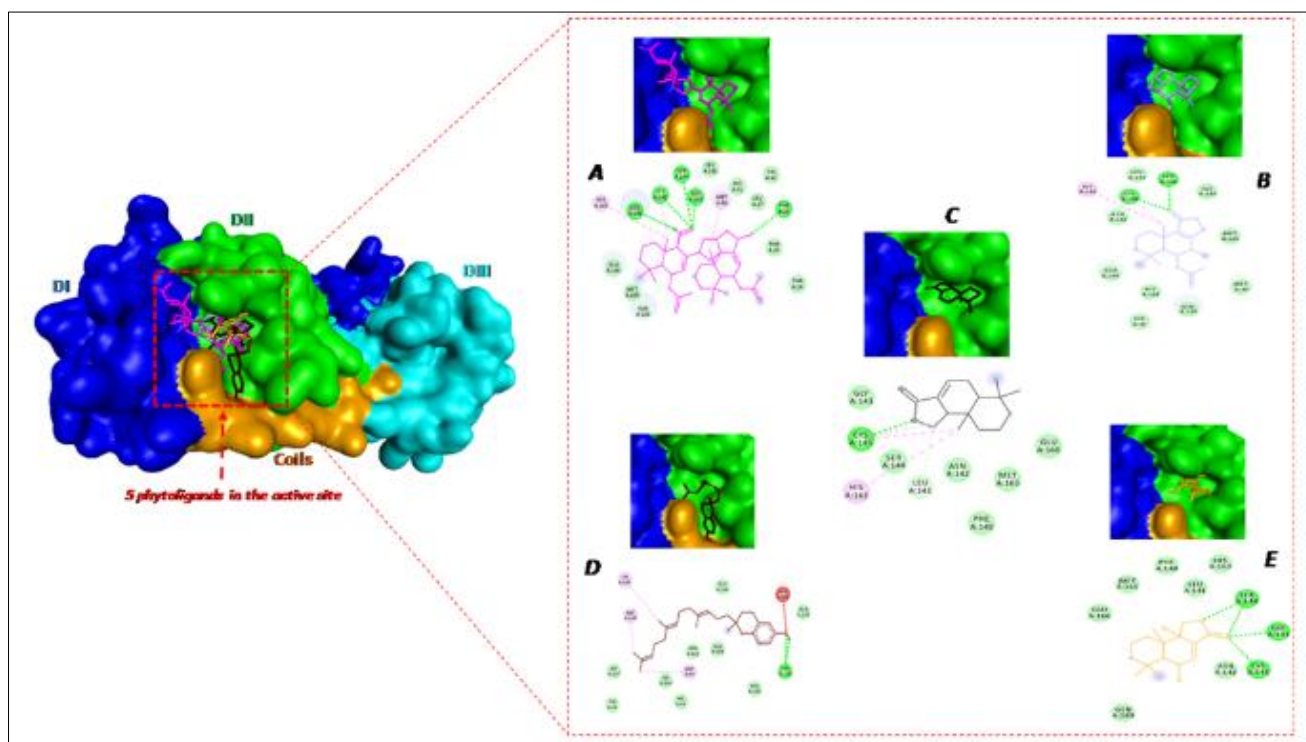


**Figure 4** Visualization of 3D and 2D interaction of 5 phytomolecules with Mpro. The subdomains of Mpro are presented in hydrophobicity while the 5 phytomolecules are presented as sticks: (A) Capsicodendrin, (B) Ugandensolide, (C) Cinnamolide, (D) Tocotrienol and (E) Pereniporin B. The different interactions modes of these phytomolecules with the residues of the active site of Mpro are also represented: hydrogen bonds, hydrophobic bonds and pi-cation bond are colored in green, purple and beige respectively. Non-favorable interactions are shown as red lines.

#### PLpro

The five selected phytomolecules are also well anchored in the active site of PLpro (Figure 5). Capsicodendrin established three hydrogen bonds with Leu<sup>162</sup>, Arg<sup>166</sup> and Tyr<sup>264</sup> and three hydrophobic bonds with Pro<sup>147</sup>, Pro<sup>148</sup> and Tyr<sup>264</sup> (Figure 5A). In addition, two hydrogen bonds with Arg<sup>166</sup>, Tyr<sup>264</sup> and three additional hydrophobic bonds with Pro<sup>147</sup>, Pro<sup>148</sup> and Tyr<sup>264</sup> were found between Ugandensolide and PLpro (Figure 5B). However, only four hydrogen bonds (Pro<sup>147</sup>, Pro<sup>148</sup> and Tyr<sup>264</sup>) were observed in the interaction between Cinnamolide and PLpro (Figure 5C). On the

other hand, three hydrogen bonds and three hydrophobic bonds were formed between Tocotrienol and PLpro, and this involves seven residues including: Pro<sup>148</sup>, Leu<sup>162</sup>, Asp<sup>164</sup>, Arg<sup>166</sup>, Pro<sup>248</sup>, Tyr<sup>264</sup> and Tyr<sup>273</sup> (Figure 5D). Finally, one hydrogen bond via Tyr<sup>273</sup> and three hydrophobic bonds via Pro<sup>148</sup> and Tyr<sup>264</sup> contributed to the stabilization of the interaction between Pereniporin B and PLpro (Figure 5E). In these results, we noticed that all phytomolecules interacted with the residues of the PLpro active site but none of the residues of the catalytic triad Cys<sup>111</sup>, His<sup>275</sup> and Asp<sup>286</sup> of this enzyme are involved in the interactions. This leads us to suggest that the 5 selected phytomolecules are non competitive inhibitors of the PLpro enzyme.

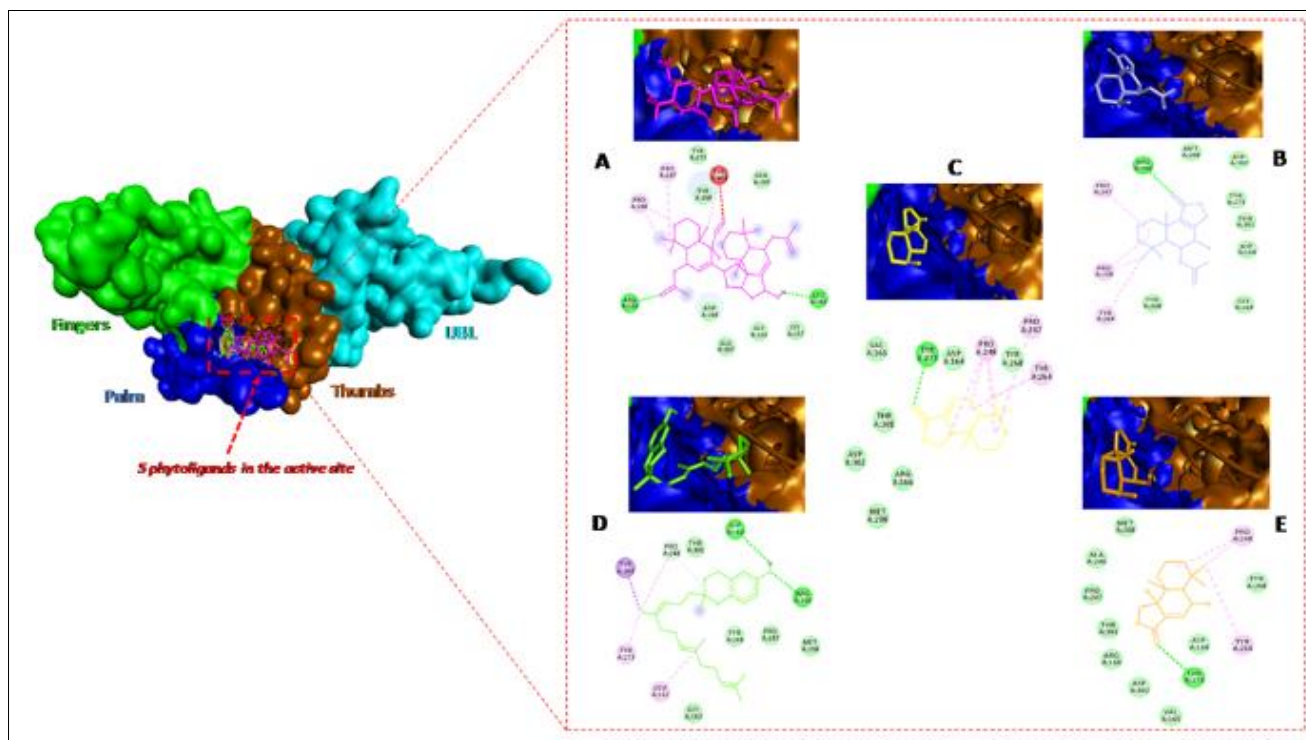


**Figure 5** Visualization of 3D and 2D interaction of 5 phytomolecules with PLpro. The subdomains of PLpro are shown in hydrophobicity, while the 5 phytomolecules are shown as sticks: (A) Capsicodendrin, (B) Ugandensolide, (C) Cinnamolide, (D) Tocotrienol and (E) Pereniporin B. The different interactions modes of these phytomolecules with the residues of the active site of the enzyme are also represented: hydrogen bonds, hydrophobic bonds and pi-cation bond are colored in green, purple and beige respectively. Non-favorable interactions are shown as red lines

### RdRp

Hydrogen and hydrophobic interactions involved the amino acids Trp<sup>800</sup>, His<sup>810</sup>, Glu<sup>811</sup>, Ser<sup>814</sup> and Lys<sup>798</sup> of the RdRp active site with Capsicodendrin (Figure 6A). Similarly, four hydrogen bonds with Trp<sup>617</sup>, Asp<sup>760</sup>, Asp<sup>761</sup>, Trp<sup>800</sup> and a hydrophobic bond with Lys<sup>798</sup> were found between Ugandensolide and RdRp (Figure 6D). In addition, hydrophobic interactions were observed between the amino acids Trp<sup>800</sup> and Lys<sup>798</sup> of the RdRp active site and Cinnamolide. Furthermore, Tocotrienol created one hydrogen bond with Trp<sup>800</sup>, and three hydrophobic bonds with Trp<sup>800</sup>, Lys<sup>798</sup> and Glu<sup>811</sup> (Figure 6D). Finally, the interaction of Pereniporin B with RdRp was only stabilized by Van Der Waals interactions (Figure 6E). These results indicate that only Ugandensolide interacted with two residues of the triadic<sup>759</sup>Ser-Asp-Asp<sup>761</sup> site of RdRp. Therefore, this phytomolecule should be a competitive inhibitor of this enzyme. The other phytomolecules such as Capsicodendrin, Cinnamolide, Tocotrienol and Pereniporin B interacted only with the other residues of the active site. They can therefore be described as non competitive inhibitors of the RdRp enzyme. Therefore, their inhibitory capacities depend on their binding energies to the enzyme.

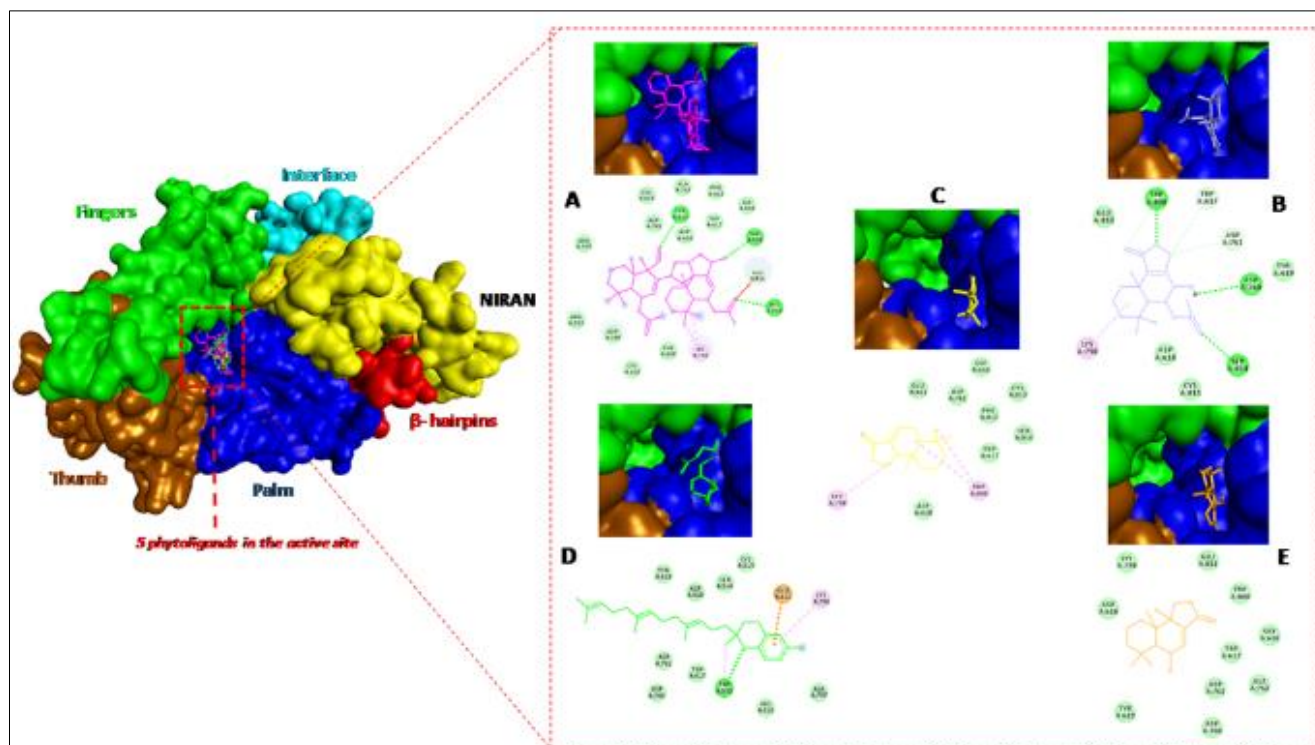


**Figure 6** Visualization of 3D and 2D interaction of 5 phytomolecules with RdRp. The subdomains of RdRp are presented in hydrophobicity while the 5 phytomolecules are presented as sticks of different colors: (A) Capsicodendrin, (B) Ugandensolide, (C) Cinnamolide, (D) Tocotrienol and (E) Pereniporin B. The different modes of interaction of these phytomolecules with the residues of the active site of the enzyme are also represented: the hydrogen bonds, the hydrophobic bonds and the pi-cation bond are colored in green, purple and beige respectively

#### Helicase

The amino acids Gly<sup>285</sup>, Lys<sup>288</sup>, Arg<sup>443</sup>, and Ala<sup>316</sup> in the active site of nsp13 are involved in the formation of three hydrogen bonds and three hydrophobic bonds with Capsicodendrin (Figure 7A). In addition, four hydrogen bonds and two hydrophobic bonds with Thr<sup>286</sup>, Gly<sup>287</sup>, Lys<sup>288</sup>, Arg<sup>443</sup> and Lys<sup>288</sup> and Ala<sup>316</sup> were found between Ugandensolide and helicase (Figure 7B). Furthermore, a hydrogen bond and an additional hydrophobic bond are found between Lys<sup>285</sup> and Ala<sup>316</sup> of the helicase and Cinnamolide (Figure 7C). We also found that Tocotrienol formed two hydrophobic bonds and one hydrophobic bond with Lys<sup>288</sup> and Ala<sup>316</sup> of the helicase (Figure 7D). Finally, pereniporin B formed a stable interaction with the helicase by forming six hydrogen bonds with Gly<sup>285</sup>, Thr<sup>286</sup>, Lys<sup>288</sup>, Ser<sup>289</sup>, Gly<sup>538</sup> and three hydrophobic bonds with Ala<sup>316</sup> (Figure 7E). All these residues that interact with phytomolecules are located in the ATP hydrolysis site of the helicase (Figure 3A). Thus, we conclude that the five phytomolecules selected in this study have the ability to inhibit the function of this enzyme by intervening at the ATP hydrolysis site.

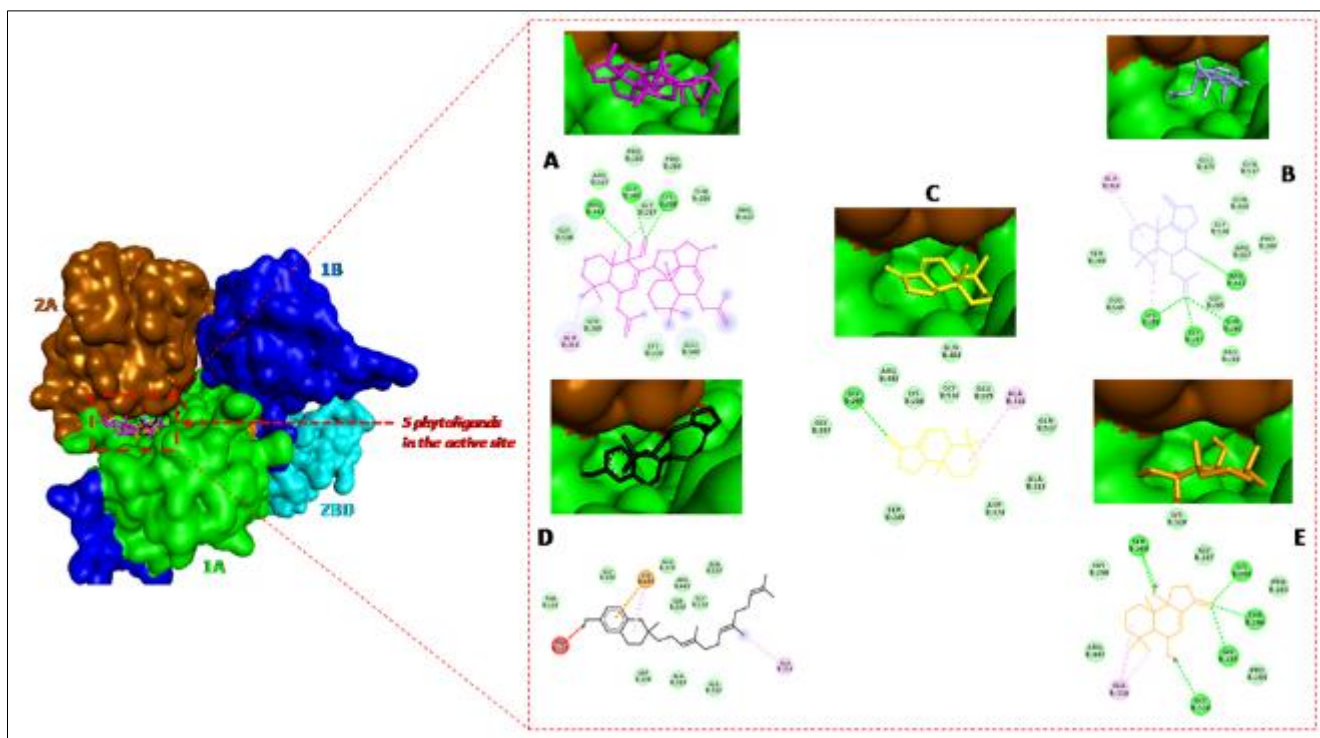


**Figure 7** Visualization 3D and 2D of interaction 5 phytomolecules with helicase: The subdomains of the helicase are presented in hydrophobicity while the 5 phytomolecules are presented as sticks of different colors: (A) Capsicodendrin, (B) Ugandensolide, (C) Cinnamolide, (D) Tocotrienol and (E) Pereniporin B. The different modes of interactions of these phytomolecules with the residues of the active site of the enzyme are also represented: hydrogen bonds, hydrophobic bonds and pi-cation bond are colored in green, purple and beige respectively. Non-favorable interactions are shown as red lines

### 2'-O-MTase

The interaction of Capsicodendrin with nsp16 involved four hydrogen bonds with Lys<sup>46</sup>, Gly<sup>71</sup>, Asn<sup>101</sup>, Asp<sup>133</sup> and three hydrophobic bonds with Leu<sup>100</sup>, Tyr<sup>132</sup>, Pro<sup>134</sup> (Figure 8A). In addition, Ugandensolide formed three hydrogen bonds with Asn<sup>43</sup>, Asn<sup>101</sup> and Asp<sup>99</sup> and two hydrophobic bonds with Tyr<sup>132</sup>, Pro<sup>134</sup> from nsp16 (Figure 8B). Concerning Cinnamolide, two hydrogen bonds and ten hydrophobic bonds engaged the amino acids Leu<sup>100</sup>, Cys<sup>115</sup> and Leu<sup>100</sup>, Cys<sup>115</sup>, Met<sup>131</sup>, Phe<sup>149</sup> for its interaction with nsp16 (Figure 8C). Furthermore, one hydrogen bond with Lys<sup>170</sup> and seven hydrophobic bonds with Leu<sup>100</sup>, Cys<sup>115</sup>, Met<sup>131</sup>, Phe<sup>149</sup> were observed between Tocotrienol and nsp16 (Figure 8D). Finally, Pereniporin B formed only one hydrophobic bond with Tyr<sup>132</sup> of nsp16 (Figure 8E).

These results indicate that the five phytomolecules selected in this study blocked the RNA binding site of nsp16 by binding with several amino acid residues of this site. However, only Capsicodendrin and Tocotrienol formed hydrogen bonds with Lys<sup>46</sup> and Lys<sup>170</sup>. Since these two residues form with Asp<sup>130</sup> and Glu<sup>203</sup> the 4 residues of the 2'-O-MTase tetrad site, we conclude that these two phytomolecules are probably effective inhibitors of nsp16.

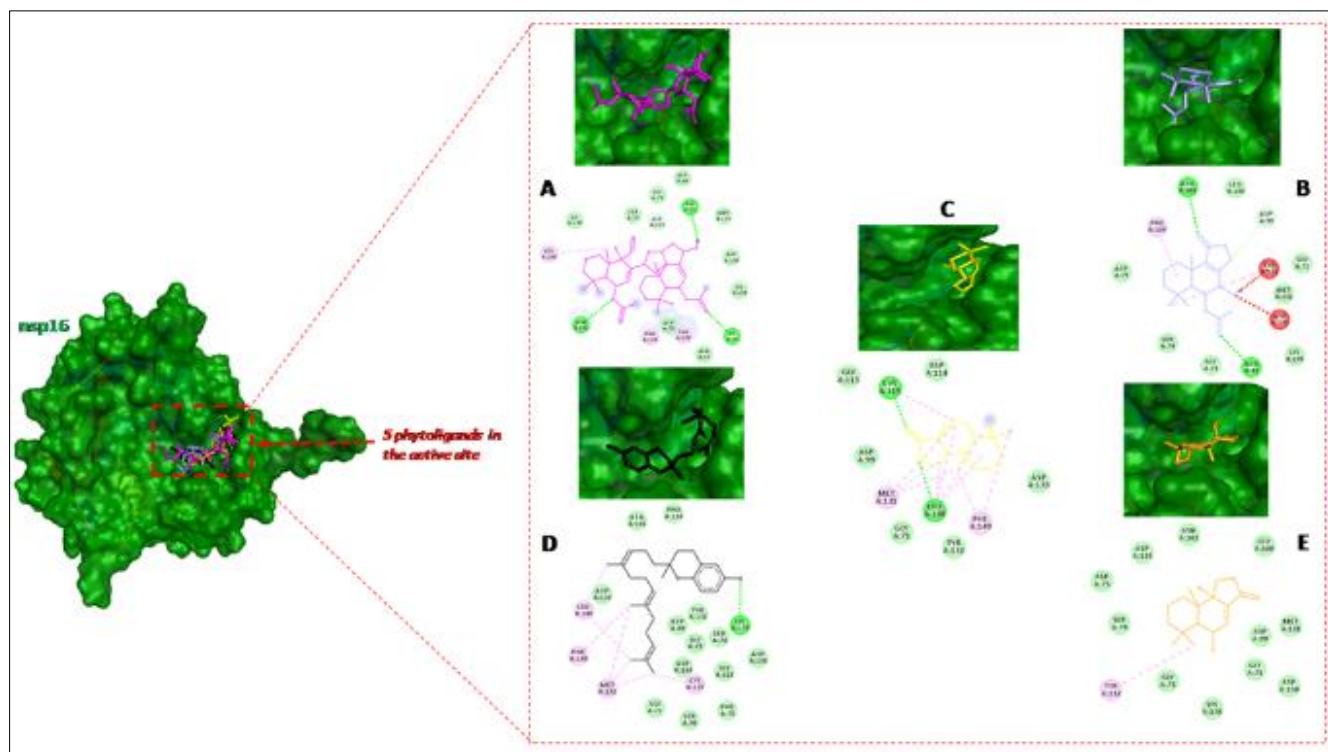


**Figure 8** Visualization 3D and 2D of interaction 5 phytomolecules with 2'-O-MTase. The 5 phytomolecules are presented as different colored sticks: (A) Capsicodendrin, (B) Ugandensolide, (C) Cinnamolide, (D) Tocotrienol and (E) Pereniporin B. The different modes of interactions of these phytomolecules with the residues of the active site of the enzyme are also represented: hydrogen bonds, hydrophobic bonds and pi-cation bond are colored in green, purple and beige respectively. Non-favorable interactions are shown as red lines

#### 4. Discussion

Since the identification of COVID-19 in China in late December 2019, scientists have continuously searched for drugs and vaccines to eradicate this disease. Many drugs have been proposed and their efficacy has already been clinically evaluated. Among these, we can mention Remdesivir [22], Chloroquine and Hydroxychloroquine [23], Lopinavir and Ritonavir [24], Azithromycin [25] and many others [26]. Several candidate vaccines have also been developed [27]. Despite these efforts, variants of SARS-CoV-2 are still identified in various countries around the world [28]. This confirms that COVID-19 will always remain a great problem for global health.

In Madagascar, the first case of COVID-19 was detected in March 2020 [29]. Since then, many people tend to use medicinal plants and their by-products (like essential oils) for the treatment and/or prevention of this disease. Examples are *Artemisia annua*, *Eucalyptus globulus*, *Allium sativum*, *Zingiber officinalis* and *Cinnamosma fragrans*. However, no conclusive research results have yet been able to prove, or even provide clear scientific explanations that these medicinal plants or their derived products contain any phytomolecules capable of treating COVID-19 or preventing SARS-CoV-2 infection. Therefore, the present study is conducted to identify phytomolecules with an inhibitory property against SARS-CoV-2 replication in some aromatics medicinal plants from Madagascar. Since *in vitro* and *in vivo* analysis processes are very expensive and time consuming, very costly and time consuming, we chose to use the molecular docking, one of bioinformatics or *in silico* method [30, 31]. Many researchers have also used this method in the search for drugs against SARS-CoV-2 [32-35].

First, we selected as ligands the seventy-six phytomolecules from sixteen aromatics medicinal plants from Madagascar (Supplementary Table 1). Most of them are monoterpenes and sesquiterpenes (Table 3). They are thus volatile compounds and major components of essential oils [36]. In addition, they are well known for their antiparasitic, antibacterial, antiviral, anti-inflammatory, and anticancer activity [37, 38]. Conversely, we chose as targets the five nsps including Mpro, PLpro, RdRp, Helicase and 2'-O-MTase of SARS-CoV-2 (Table 1). These nsps are very important in the replication of SARS-CoV-2 and are also highly conserved in these viruses [8, 9, 39, 40]. In addition, they are constantly

targeted in the search for drugs against COVID-19 [41-46]. Together, the selection of ligands and targets correspond greatly with the objective of this study, and also with the use of these plants in the COVID-19 pandemic.

Then, we predicted the active site residues of these five target nsps. In result, twenty-one amino acid residues are predicted in the active site of MPro (Figure 1A). This result is comparable to the results reported by other researchers [47, 48]. In contrast, eleven residues are predicted in the active site of PLpro (Figure 1B) and we did not predict the residues of the catalytic triad site (Cys<sup>111</sup>, His<sup>272</sup> and Asp<sup>286</sup>) described by Osipiuk and colleagues [49]. However, this triadic site is not considered a potential target in the search for PLpro inhibitors [50]. Similarly, we did not predict the four key residues (D<sup>618</sup>, S<sup>759</sup>, D<sup>760</sup> and D<sup>761</sup>) of the active site of RdRp [14]. Nevertheless, we predicted five residues (Pro<sup>809</sup>, Glu<sup>811</sup>, Phe<sup>812</sup>, Cys<sup>813</sup> and Ser<sup>814</sup>) that are very close to these key residues (Figure 2). Thus, the non-prediction of these keys residues has no effect on the docking results. In addition, we found sixteen residues, which are located in the ATP hydrolysis site and in the DNA binding site of the helicase (Figure 3A). These two sites are generally considered to be potential drug binding sites in helicase [15]. Finally, we predicted eighteen residues that localize in the RNA binding site and SAM binding site of 2'-O-MTase (Figure 3B). Krafcikova and colleagues have previously reported that these two sites could be targeted in the search for inhibitors of this enzyme [16].

Finally, we performed molecular docking. We found that only five drimane sesquiterpenes (Capsicodendrin, Ugandensolide, Cinnamolide, Tocotrienol, and Pereniporin B) interacted strongly with the five target nsps and were able to inhibit their functions (Table 5 and Figure 4, 5, 6, 7 and 8). Surprisingly, these are all secondary metabolites of *Cinnamosma fragrans* [51-53]. This plant is one of the endemic medicinal plants of Madagascar and is well known by its name of "*Mandravasarotra*, *Saro* and *Sakarivohazo*" [53]. Traditionally, it is used to treat respiratory problems [54]. A decoction of its bark is also used to treat muscle pain and symptoms of malaria [52]. In addition, its essential oil is well known for its antimicrobial properties [55] and for its use in the treatment of otorhinolaryngological diseases [54]. Recently, Pidoux and his colleagues have further indicated that the essential oils of this plant have an anti-inflammatory properties [56]. These numerous pharmacological effects have inspired the Malagasy to give its name to "*Mandravasarotra*", which literally means "those who fight everything". These numerous properties have also motivated many Malagasy to use it in the treatment of various infectious diseases, including COVID-19.

In this *in silico* study, these five were found to be inhibitors of 5 nsps of SARS-CoV-2 (Table 4 and Figures 4, 5, 6, 7, and 8). Bearing in mind, previous studies have reported that Capsicodendrin, Ugandensolide, Cinnamolide, and Pereniporin B are  $\alpha$ -glucosidase inhibiting agents[57]. Tocotrienol is reported to be a rare form of vitamin E [58]. But Williams and colleagues still indicated that  $\alpha$ -glucosidase inhibitors have the potential to inhibit SARS-CoV-2 replication [59]. For their part, Samad and colleagues also reported that vitamins A, D, E, and K may boost immune defenses and prevent complications of COVID-19, such as cytokine storm [60]. Therefore, the five phytomolecules identified in this study may be both possible inhibitors of SARS-CoV-2 replication and may also have immunomodulatory effects.

---

## 5. Conclusion

In summary, this docking study revealed that Capsicodendrin, Ugandensolide, Cinnamolide, Tocotrienol and Pereniporin B from *Cinnamosma fragrans* or "*Mandravasarotra*, in Malagasy" can inhibit the five non-structural proteins of SARS-CoV-2. Thus, these phytomolecules may have the capacity to inhibit replication of these viruses. Given the previous knowledge of the various pharmacological properties of *Cinnamosma fragrans*, we can suggest that further analysis of these phytomolecules offers a new perspective in the research for antiviral drugs against COVID-19. Thus, further *in vitro* and *in vivo* studies are still needed to valorize these results.

---

## Compliance with ethical standards

### *Acknowledgments*

We thank the Malagasy Institute of Veterinary Vaccines (IMVAVET) for supplying the required equipment for this study.

### *Disclosure of conflict of interest*

The authors declare that they have no competing interests.

### *Funding*

No specific funding was received for this study.

*Authors' contributions*

T.R. performed all molecular work and wrote the manuscript. F.O.M. supervised the realization of this work. All authors have read and approved the final manuscript.

**References**

- [1] Song F, Shi N, Shan F, Zhang Z, Shen J, Lu H, Ling Y, Jiang Y, Shi Y. Emerging 2019 Novel Coronavirus (2019-nCoV) Pneumonia. *Radiology*. 2020; 295(1):210-217.
- [2] Zhu H, Wei L, Niu P. The novel coronavirus outbreak in Wuhan, China. *Global health research and policy*. 2020; 5(1):1-3.
- [3] Arnaout R, Arnaout R. Visualizing omicron: COVID-19 deaths vs. cases over time. *PLoS One*. 2022; 17(4):e0265233.
- [4] Villena-Tejada M, Vera-Ferchau I, Cardona-Rivero A, Zamalloa-Cornejo R, Quispe-Florez M, Frisancho-Triveño Z, Abarca-Meléndez RC, Alvarez-Sucari SG, Mejia CR, Yañez JA. Use of medicinal plants for COVID-19 prevention and respiratory symptom treatment during the pandemic in Cusco, Peru: A cross-sectional survey. *PLoS One*. 2021; 16(9):e0257165.
- [5] Popoola TD, Segun PA, Ekuadzi E, Dickson RA, Awotona OR, Nahar L, Sarker SD, Fatokun AA. West African medicinal plants and their constituent compounds as treatments for viral infections, including SARS-CoV-2/COVID-19. *Daru*. 2022; 30(1):191-210.
- [6] Demeke CA, Woldeyohanins AE, Kifle ZD. Herbal medicine use for the management of COVID-19: A review article. *Metabolism Open*. 2021; 12:100141.
- [7] Sharma V, Sarkar IN. Bioinformatics opportunities for identification and study of medicinal plants. *Brief Bioinform*. 2013; 14(2):238-250.
- [8] Liu XH, Zhang X, Lu ZH, Zhu YS, Wang T. Potential molecular targets of nonstructural proteins for the development of antiviral drugs against SARS-CoV-2 infection. *Biomedicine & Pharmacotherapy*. 2021; 133:111035.
- [9] Yadav R, Chaudhary JK, Jain N, Chaudhary PK, Khanra S, Dhamija P, Sharma A, Kumar A, Handu S. Role of Structural and Non-Structural Proteins and Therapeutic Targets of SARS-CoV-2 for COVID-19. *Cells*. 2021, 10(4):821
- [10] Biovia, Dassault Systèmes, Discovery Studio Visualizer, Release 2017, San Diego: Dassault Systèmes, 2017.
- [11] Wang J, Wang W, Kollman PA, Case DA. Automatic atom type and bond type perception in molecular mechanical calculations. *J Mol Graph Model*. 2006; 25(2):247-260.
- [12] Jin Z, Du X, Xu Y, Deng Y, Liu M, Zhao Y, and al. Structure of Mpro from SARS-CoV-2 and discovery of its inhibitors. *Nature*. 2020; 582(7811):289-293.
- [13] Rut W, Lv Z, Zmudzinski M, Patchett S, Nayak D, Snipas SJ, El Oualid F, Huang TT, Bekes M, Drag M, Olsen SK. Activity profiling and crystal structures of inhibitor-bound SARS-CoV-2 papain-like protease: A framework for anti-COVID-19 drug design. *Sci Adv*. 2020; 6(42):eabd4596.
- [14] Gao Y, Yan L, Huang Y, Liu F, Zhao Y, and al. Structure of the RNA-dependent RNA polymerase from COVID-19 virus. *Science*. 2020; 368(6492):779-782.
- [15] Newman JA, Douangamath A, Yadzani S, Yosaatmadja Y, Aimon A, Brandão-Neto J, Dunnett L, Gorrie-Stone T, Skyner R, Fearon D, Schapira M, von Delft F, Gileadi O. Structure, mechanism and crystallographic fragment screening of the SARS-CoV-2 NSP13 helicase. *Nat Commun*. 2021; 12(1):4848.
- [16] Krafcikova P, Silhan J, Nencka R, Boura E. Structural analysis of the SARS-CoV-2 methyltransferase complex involved in RNA cap creation bound to sinefungin. *Nat Commun*. 2020; 11(1):3717.
- [17] Wu Q, Peng Z, Zhang Y, Yang J. COACH-D: improved protein-ligand binding sites prediction with refined ligand-binding poses through molecular docking. *Nucleic Acids Res*. 2018; 46(W1):438- 442.
- [18] Dallakyan S, Olson A. Small-Molecule Library Screening by Docking with PyRx. *Methods Mol Biol*. 2015; 1263:243-250.
- [19] O'Boyle NM, Banck M, James CA, Morley C, Vandermeersch T, Hutchison GR. Open Babel: An open chemical toolbox. *J Chem Inform*. 2011; 3(1):33.

- [20] Morris GM, Goodsell DS, Halliday RS, Huey R, Hart WE, Belew RK, Olson AJ. Automated docking using a Lamarckian genetic algorithm and an empirical binding free energy function. *J Comput Chem*. 1998; 19(14):1639-1662.
- [21] Trott O, Olson AJ. AutoDock Vina: Improving the speed and accuracy of docking with a new scoring function, efficient optimization, and multithreading. *J Comput Chem*. 2010; 31(2):455-461.
- [22] Beigel JH, Tomashek KM, Dodd LE, Mehta AK, Zingman BS, Kalil AC, et al. Remdesivir for the Treatment of Covid-19 — Final Report. *N Engl J Med*. 2020; 383(19):1813-1826.
- [23] Ren L, Xu W, Overton JL, Yu S, Chiamvimonvat N, Thai PN. Assessment of Chloroquine and Hydroxychloroquine Safety Profiles: A Systematic Review and Meta-Analysis. *Front Pharmacol*. 2020; 11(1584):562777.
- [24] Patel TK, Patel PB, Barvaliya M, Saurabh MK, Bhalla HL, Khosla PP. Efficacy and safety of lopinavir-ritonavir in COVID-19: A systematic review of randomized controlled trials. *J Infect Public Health*. 2021; 14(6):740-748.
- [25] Gautret P, Lagier J-C, Parola P, Hoang VT, Meddeb L, Mailhe M, Doudier B, Courjon J, Giordanengo V, Vieira VE, Tissot Dupont H, Honoré S, Colson P, Chabrière E, La Scola B, Rolain JM, Brouqui P, Raoult D. Hydroxychloroquine and azithromycin as a treatment of COVID-19: results of an open-label non-randomized clinical trial. *Int J Antimicrob Agents*. 2020; 56(1):105949.
- [26] De P, Chakraborty I, Karna B, Mazumder N. Brief review on repurposed drugs and vaccines for possible treatment of COVID-19. *Eur J Pharmacol*. 2021; 898:173977.
- [27] Li Y, Tenchov R, Smoot J, Liu C, Watkins S, Zhou Q. A Comprehensive Review of the Global Efforts on COVID-19 Vaccine Development. *ACS Cent Sci*. 2021; 7(4):512-533.
- [28] Banoun H. Evolution of SARS-CoV-2: Review of Mutations, Role of the Host Immune System. *Nephron Clin Pract*. 2021; 145(4):392-403.
- [29] Randremanana RV, Andriamandimby SF, Rakotondramanga JM. The COVID-19 epidemic in Madagascar: clinical description and laboratory results of the first wave, march-september 2020. *Influenza and other respiratory viruses*. 2021; 15(4):457-468.
- [30] Abubakar AR, Haque M. Preparation of Medicinal Plants: Basic Extraction and Fractionation Procedures for Experimental Purposes. *J Pharm Bioallied Sci*. 2020; 12(1):1.
- [31] Yi F, Li L, Xu LJ, Meng H, Dong YM, Liu HB, Xiao PG. *In silico* approach in reveal traditional medicine plants pharmacological material basis. *Chin Med*. 2018; 13:33-33.
- [32] Elmi A, Sayem SA-J, Ahmed M, Abdoul-Latif F. Natural compounds from djiboutian medicinal plants as inhibitors of covid-19 by *in silico* investigations. *International Journal of Current Pharmaceutical Research*. 2020; 12(4):52-57.
- [33] Jamali N, Soureshjani EH, Mobini GR, Samare-Najaf M, Clark CT, Saffari-Chaleshtori J. Medicinal plant compounds as promising inhibitors of coronavirus (COVID-19) main protease: an *in silico* study. *Journal of Biomolecular Structure and Dynamics*. 2021:1-12.
- [34] Elmaaty AA, Darwish KM, Khattab M, Elhady SS, Salah M, Hamed MIA, Al-Karmalawy AA, Saleh MM. In a search for potential drug candidates for combating COVID-19: computational study revealed salvianolic acid B as a potential therapeutic targeting 3CLpro and spike proteins. *Journal of Biomolecular Structure and Dynamics*. 2021:1-28.
- [35] S Shree P, Mishra P, Selvaraj C, Singh SK, Chaube R, Garg N, Tripathi YB. Targeting COVID-19 (SARS-CoV-2) main protease through active phytochemicals of ayurvedic medicinal plants – *Withania somnifera* (Ashwagandha), *Tinospora cordifolia* (Giloy) and *Ocimum sanctum* (Tulsi) – a molecular docking study. *Journal of Biomolecular Structure and Dynamics*. 2022; 40(1):190–203.
- [36] Buckle J. Basic Plant Taxonomy, Basic Essential Oil Chemistry, Extraction, Biosynthesis, and Analysis. *Clinical aromatherapy*. 2015:37-72.
- [37] Swamy MK, Akhtar MS. Antimicrobial Properties of Plant Essential Oils against Human Pathogens and Their Mode of Action: An Updated Review. *Evidence-Based Complementary and alternative medicine*. 2016:3012462.
- [38] Cox-Georgian D, Ramadoss N, Dona C, Basu C. Therapeutic and Medicinal Uses of Terpenes. In: *Medicinal Plants*; Springer, Cham; 2019. p. 333-359.



- [39] Chaudhuri D, Majumder S, Datta J, Giri K. *In Silico* Study of Mutational Stability of SARS-CoV-2 Proteins. *Protein J*. 2021; 40(3):328-340.
- [40] Sarkar R, Mitra S, Chandra P, Saha P, Banerjee A, Dutta S, Chawla-Sarkar M. Comprehensive analysis of genomic diversity of SARS-CoV-2 in different geographic regions of India: an endeavour to classify Indian SARS-CoV-2 strains on the basis of co-existing mutations. *Arch Virol*. 2021; 166(3):801-812.
- [41] Kumar V, Parate S, Yoon S, Lee G, Lee KW. Computational Simulations Identified Marine-Derived Natural Bioactive Compounds as Replication Inhibitors of SARS-CoV-2. *Frontiers in microbiology*. 2021; 12(583).
- [42] Thurakkal L, Singh S, Roy R, Kar P, Sadhukhan S, Porel M. An *in silico* study on selected organosulfur compounds as potential drugs for SARS-CoV-2 infection via binding multiple drug targets. *Chemical physics letters*. 2021; 763:138193.
- [43] Prajapat M, Sarma P, Shekhar N, Avti P, Sinha S, Kaur H, Kumar S, Bhattacharyya A, Kumar H, Bansal S, Medhi B. Drug targets for corona virus: A systematic review. *Indian J Pharmacol*. 2020; 52(1):56-65.
- [44] Spratt AN, Gallazzi F, Quinn TP, Lorson CL, Sönnnerborg A, Singh K. Coronavirus helicases: attractive and unique targets of antiviral drug-development and therapeutic patents. *Expert Opin Ther Pat*. 2021; 31(4):339-350.
- [45] Shu T, Gan T, Bai P, Wang X, Qian Q, Zhou H, Cheng Q, Qiu Y, Yin L, Zhong J, Zhou X. Ebola virus VP35 has novel NTPase and helicase-like activities. *Nucleic Acids Res*. 2019; 47(11):5837-5851.
- [46] Wang Y, Sun Y, Wu A, Xu S, Pan R, Zeng C, Jin X, Ge X, Shi Z, Ahola T, Chen Y, Guo D. Coronavirus nsp10/nsp16 Methyltransferase Can Be Targeted by nsp10-Derived Peptide *In Vitro* and *In Vivo* To Reduce Replication and Pathogenesis. *J Virol*. 2015; 89(16):8416-8427.
- [47] Gahlawat A, Kumar N, Kumar R, Sandhu H, Singh IP, Singh S, Sjöstedt A, Garg P. Structure-Based Virtual Screening to Discover Potential Lead Molecules for the SARS-CoV-2 Main Protease. *J Chem Inf Model*. 2020; 60(12):5781-5793.
- [48] Zhu J, Zhang H, Lin Q, Lyu J, Lu L, Chen H, Zhang X, Zhang Y, Chen K. Progress on SARS-CoV-2 3CLpro Inhibitors: Inspiration from SARS-CoV 3CLpro Peptidomimetics and Small-Molecule Anti-Inflammatory Compounds. *Drug Des Devel Ther*. 2022; 16:1067-1082.
- [49] Osipiuk J, Azizi S-A, Dvorkin S, Endres M, Jedrzejczak R, Jones KA, et al. Structure of papain-like protease from SARS-CoV-2 and its complexes with non-covalent inhibitors. *Nat Commun*. 2021; 12(1):743.
- [50] Shen Z, Ratia K, Cooper L, Kong D, Lee H, Kwon Y, Li Y, Alqarni S, Huang F, Dubrovskiy O, Rong L, Thatcher G, Xiong R. Design of SARS-CoV-2 PLpro Inhibitors for COVID-19 Antiviral Therapy Leveraging Binding Cooperativity. *J Med Chem*. 2022; 65(4):2940-2955.
- [51] Canonica L, Corbella A, Jommi G, Křepinský J, Ferrari G, Casagrande C. The structure of cinnamolide, cinnamosmolide and cinnamodial, sesquiterpenes with drimane skeleton from *Cinnamosma fragrans* baillon. *Tetrahedron Letters*. 1967; 8(23):2137-2141.
- [52] Harinantenaina L, Takaoka S. Cinnafagrins A–C, Dimeric and Trimeric Drimane Sesquiterpenoids from *Cinnamosma fragrans*, and Structure Revision of Capsicodendrin. *J Nat Prod*. 2006; 69(8):1193-1197.
- [53] Quéro A, Molinié R, Brancourt D, Rémy MJ, Mesnard F. Sesquiterpene composition of *Cinnamosma fragrans*: A Malagasy endemic plant used in traditional medicine. *Comptes Rendus Chimie*. 2016; 19(9):1056-1061.
- [54] Randrianarivelo R, Sarter S, Odoux E, Brat P, Lebrun M, Romestand B, Menut C, Andrianoelisoa HS, Raheimandimby M, Danthu P. Composition and antimicrobial activity of essential oils of *Cinnamosma fragrans*. *Food Chemistry*. 2009; 114(2):680-684.
- [55] Behra O, Danthu P, Sarter S, Radaniela R, Fourcade C, Randrianarivelo R, Ranaivosoa B, Arnal-Schnebel B. Saro (*Cinnamosma fragrans* Baillon) essential oil: Application in Health and Medicine. In: Juliani H, Rodolfo, Simon JE, Ho Chi-Tang, editors. African natural plant products: new discoveries and challenges in chemistry and quality. Washington: ACS, 2009. p. 485-494.
- [56] Pidoux M, Harilalarisoa H, Iharilanto R, Rabenoavy M, Rakotondramanana R, Ravaoarinirina S, Andriambolona-Voahangy D. Prévention des infections postopératoires superficielles et cicatrisation des lésions à l'aide d'un mélange d'huiles de Saro et de *Calophyllum inophyllum*: cas des circoncisions à Madagascar. *Phytothérapie*. 2012; 10: 143–147.

- [57] Harinantenaina L, Matsunami K, Otsuka H, Kawahata M, Yamaguchi K, Asakawa Y. Secondary metabolites of *Cinnamosma madagascariensis* and their alpha-glucosidase inhibitory properties. *J Nat Prod.* 2008; 71(1):123-126.
- [58] Theriault A, Chao JT, Wang Q, Gapor A, Adeli K. Tocotrienol: a review of its therapeutic potential. *Clin Biochem.* 1999; 32(5):309-319.
- [59] Williams SJ, Goddard-Borger ED.  $\alpha$ -glucosidase inhibitors as host-directed antiviral agents with potential for the treatment of COVID-19. *Biochem Soc Trans.* 2020; 48(3):1287-1295.
- [60] Samad N, Dutta S, Sodunke TE, Fairuz A, Sapkota A, Miftah ZF, Jahan I, Sharma P, Abubakar AR, Rowaiye AB, Oli AN, Charan J, Islam S, Haque M. Fat-Soluble Vitamins and the Current Global Pandemic of COVID-19: Evidence-Based Efficacy from Literature Review. *J Inflamm Res.* 2021; 14:2091-2110.
- [61] Manda A. Contribution à l'étude de l'huile essentielle de *Vetiveria zizanioides stapf* (gramineae) variabilité de la composition chimique selon la zone de récolte [CAPEN: Mémoire de fin d'étude]. ENS: Université d'Antananarivo; 2005.
- [62] Noëlla RF. Contribution à l'étude des impacts des maladies de plante sur les huiles d'Eucalyptus dans la région Analamanga: *Eucalyptus citriodora* et *Eucalyptus globulus* (MYRTACEAE) [ING. Mémoire de fin d'étude]. ESSA: Université d'Antananarivo; 2015.
- [63] Lancia RL. Valorisation du Gingembre de Beforona en huile essentielle et oleoresine : Cas de la société BIOSAVE: Optimisation du rendement et contrôle qualité [ING. Mémoire de fin d'étude]. ESSA: Université d'Antananarivo; 2005.
- [64] Mbolanirina AS. Contribution a l'étude de l'huile essentielle de gingembre en vue d'une meilleure exploitation [ING. Mémoire de fin d'étude]. ESPA: Université d'Antananarivo; 2010.
- [65] Tojonilaina RDF. Etude des effets de traitement sylvicole sur l'évolution des chemotypes d'huile essentielle de *Ravensara aromatica* des forêts dans le corridor *Zahamena mantadia* [ING. Mémoire de fin d'étude]. ESSA: Université d'Antananarivo; 2008.
- [66] Rouf R, Uddin SJ, Sarker DK, Islam MT, Ali ES, Shilpi JA, et al. Antiviral potential of garlic (*Allium sativum*) and its organosulfur compounds: A systematic update of pre-clinical and clinical data. *Trends in food science & technology.* 2020; 104:219-234.
- [67] Diamondra MN. Huiles essentielles d'*Ocimum gratissimum*: Extraction et formulation d'un baume [Master. Mémoire de fin d'étude]. Faculté des sciences: Université d'Antananarivo; 2021.
- [68] Chalchat JC, Valade I. Chemical Composition of Leaf Oils of *Cinnamomum* from Madagascar: *C. zeylanicum* Blume, *C. camphora* L., *C. fragrans* Baillon and *C. angustifolium*. *Journal of Essential Oil Research.* 2000; 12(5):537-540.
- [69] Ramanoelina PAR, Bianchini JP, Andriantsiferana M, Viano J, Gaydou EM. Chemical Composition of Niaouli Essential Oils from Madagascar. *Journal of Essential Oil Research.* 1992; 4(6):657-658.
- [70] Afoulous S, Ferhout H, Raoelison EG, Valentin A, Moukarzel B, Couderc F, et al. Chemical composition and anticancer, anti-inflammatory, antioxidant and antimalarial activities of leaves essential oil of *Cedrelopsis grevei*. *Food and Chemical Toxicology.* 2013; 56:352-362.
- [71] Cavalli J-F, Tomi F, Bernardini A-F, Casanova J. Composition and chemical variability of the bark oil of *Cedrelopsis grevei* H. Baillon from Madagascar. *Flavour and Fragrance Journal.* 2003; 18(6):532-538.
- [72] Dominique HNMO. Etudes préliminaires de la composition de la composition chimique de l'huile essentielle de *Schinus terebenthifolius* et de leurs activités biologique [ING. Mémoire de fin d'étude]. ESSA: Université d'Antananarivo; 2006.
- [73] Alex AM. Contribution à l'identification au laboratoire des facteurs influencant le rendement et la composition chimique en huile essentielle de *Pelargonium roseum* (Geraniaceae) : Cas de la Ferme AGRICO de Betampona [ING. Mémoire de fin d'étude]. ESSA: Université d'Antananarivo; 2008.
- [74] Cavalli JF. Caractérisation par CPG/IK, CPG/SM et RMN du carbone-13 d'huiles essentielles de Madagascar [Ph.D. Dissertation]. Autre: Université Pascal Paoli; 2002.

## Appendix

### Appendix 5 The plants and the secondary metabolites (or phytomolecules) used in this study

N° plant	Medicinal plant	Nom vernaculaire	Phytomolecules	Quantity in Percentage (%)	CID Pubchem	References
1	<i>Eucalyptus globulus</i>	<i>Kininim-potsy</i>	1,8 cineol	68 – 84.64	46781028	61, 62
			$\alpha$ -pinene	10.20 - 17	6654	
			Camphene	23.1	6616	
			Globulol	1.39- 7.3	101716	
			Limonene	0.63	22311	
			$\beta$ -pinene	0.1 – 2.7	14896	
			$\alpha$ - terpinenol	1 – 5.8	442501	
			p-cymene	0.78 – 1.2	7463	
2	<i>Zingiber officinale</i>	<i>Sakamalao</i>	$\alpha$ -pinene	5.15	6654	63, 64
			Camphene	13.82	6616	
			Zingerone	Inc.*	31211	
			Trans-6- shogaol	1.74	5281794	
			Borneol	5.6	64685	
			Geraniol	0.60 – 1.56	637566	
			Decanal	Inc.	8175	
			Gingerdiol	Inc.	11369949	
			Methyl diacetoxy-6-gingerdiol	Inc.	5319662	
			Geranial	3.20 – 3.42	638011	
			$\beta$ -phellandrene	3. 75– 4.9	11142	
			Limonene	2.72	22311	
			Sabinene	1.54	18818	
3	<i>Ravensara aromatica</i>	<i>Havozo</i>	Limonene	0 – 34.7	22311	65
			Sabinene	0 – 28.3	18818	
			Methyl chavicol	0 – 83.8	8815	
			Methyl eugenol	0 – 95.4	7127	
			Germacrene D	0 – 5.6	5317570	
			$\gamma$ -terpinene	0 – 7.2	7461	
			$\alpha$ -pinene	0 – 15.9	6654	
			$\Delta$ -3-Carene	0 - 31	443156	
4	<i>Allium sativum</i>	<i>Tongolo gasy</i>	Alliin	Inc.	87310	66
			Allicin	Inc.	65036	
			(Z)-ajoene	Inc.	9881148	
			(E)-Ajoene	Inc.	5386591	

			Isoalliin	Inc.	5281112	
			Diallyl disulfide	Inc.	16590	
			Diallyl trisulfide	Inc.	16315	
5	<i>Ocinum gratissimum</i>	<i>Romba</i>	Eugenol	68.58	3314	67
			$\beta$ -selinene	2.82	442393	
			Thymol	5.3 - 28	6989	
			$\gamma$ -terpinene	0.26	7461	
			$\beta$ -caryophyllene	1.47 - 2.03	6429274	
			Methyl eugenol	1.09	7127	
			Germacrene D	5.53	5317570	
			1,8 cineol	9.34 - 9.69	46781028	
6	<i>Cinnamosma fragrans</i>	<i>Mandravasarotra</i>	1,8 cineol	28	46781028	68
			$\alpha$ -pinene	8	6654	
			$\beta$ -pinene	10	14896	
			$\beta$ -caryophyllene	13	6429274	
			Cinnamodial	Inc.	442354	
			Pereniporin B	Inc.	161192	
			Ugandensolide	Inc.	12444581	
			Capsicodendrin	Inc.	44419494	
			Tocotrienol	Inc.	9929901	
			Cinnamolide	Inc.	12303261	
7	<i>Cinnamomum camphora</i>	<i>Ravintsara</i>	1,8 cineol	58 - 63	46781028	61, 68
			Linalool	10	6549	
			Sabinene	11 - 14	18818	
			$\alpha$ -pinene	3 - 4.5	6654	
			$\beta$ -pinene	2.5 - 3.3	14896	
			$\beta$ -terpineol	7 - 9	8748	
			$\beta$ -phellandrene	59.9	11142	
			$\gamma$ -terpinene	3.8	7461	
			Camphene	15.9	6616	
8	<i>Melaleuca quinquenevia</i>	<i>Niaouli</i>	1,8 cineol	46 - 60	46781028	69
			Linalool	50	6549	
			Nerolidol	30 - 70	5284507	
			Methyl eugenol	99	7127	
			Methyl isoeugenol	88	7128	
			Viridiflorol	48	11996452	
			$\alpha$ -thujene	5,43	17868	
9		<i>Katrafay</i>	$\beta$ -selinene	4.5	442393	

	<i>Cidrelopsis grevei</i>		$\alpha$ -pinene	2.1 -30	6654	70, 71
			Copaborneol	4.7 - 20	101289803	
			Ishwarane	1 – 17.4	14619932	
			$\Delta$ - Cadinene	4.9 - 14.48	3032853	
			T-Muurolol	11.8	3084331	
			$\alpha$ -cadinol	6.7	10398656	
			$\beta$ -elemene	6.96 – 9.6	6918391	
			$\beta$ - caryophyllene	9.3 – 12.5	6429274	
10	<i>Schinus terebenthifolius</i>	<i>Poivre</i>	$\alpha$ -phellandrene	1.08 - 15	7460	72
			$\Delta$ -3-Carene	1.10- 40.06	443156	
			$\beta$ -phellandrene	1.4 – 11.70	11142	
			$\alpha$ -pinene	2.3 – 20.76	6654	
			$\beta$ -pinene	7 - 27	14896	
			Germacrene D	0.25 – 5.14	5317570	
			$\beta$ - caryophyllene	1.41 – 22.97	6429274	
			p-cymene	0.31 – 13.83	7463	
			$\gamma$ -terpinene	0.47 – 10.55	7461	
11	<i>Pelargonium roseum</i>	<i>Geranium</i>	Linalool	3.46 – 5.57	6549	73
			Isomenthone	6.31 – 8.72	6986	
			Citronellyl formate	3.24 – 12.94	7778	
			Geranyl formate	9.26 - 11.79	5282109	
			Nerol	5.6 - 6	643820	
			Citronellol	15.84 – 16.02	8842	
			Geraniol	10.74 – 12.94	637566	
			6,9-Guaiadiene	7.2 -8.1	527113	
			Geranyl propanoate	4.27 – 4.55	5355853	
			Geranyl tiglate	2.93 – 3.68	5367785	
12	<i>Helichrysum gymnocephalum</i>	<i>Rambiazina vavy</i>	1,8 cineol	25.55- 47.4	46781028	61
			$\alpha$ -pinene	8.84	6654	
			Camphene	12.15	6616	
			$\beta$ - caryophyllene	8.93	6429274	
			Bicyclosquiphellandrene	5	521496	
			Bicyclogermacrene	5	13894537	
			$\alpha$ - terpineol	41.16	17100	
			$\alpha$ -amorphene	5.1	12306052	
			$\gamma$ -Curcumene	5.6	12304273	

13	<i>Cupressus lusitanica</i>	<i>Cyprès</i>	$\alpha$ -pinene	17.3 – 19.3	6654	74
			$\Delta$ -3-Carene	13.8 – 18.1	443156	
			Sabinene	9.4 – 19.5	18818	
			Myrcene	3.5	31253	
			Limonene	6.8	22311	
			1,8 cineol	2.39	46781028	
			p-cymene	2 – 4.8	7463	
			Isoterpinene	2.49	11463	
			Bornyl acetate	2.76	93009	
			Camphene	3.7 – 4.2	6616	
			$\alpha$ -thujene	1.3	17868	
14	<i>Pipper nigrum</i>	<i>Dipoivatra</i>	$\alpha$ -pinene	5.96- 16.3	6654	61
			$\beta$ -pinene	15.7	14896	
			Sabinene	11.71	18818	
			$\Delta$ -3-Carene	8.9- 12.7	443156	
			Limonene	15.7 – 25.9	22311	
			$\beta$ - caryophyllene	4.3- 24.86	6429274	
			Eugenol	4.2	3314	
16	<i>Citrus aurantifolia</i>	<i>Voasary makirana</i>	Limonene	79.37	22311	61
			Trans carveol	Inc.	94221	
			Cis Ocimene	Inc.	5369951	
			Linalyl acetate	Inc.	8294	
			$\beta$ - caryophyllene	Inc.	6429274	
			$\alpha$ - phellandrene	Inc.	7460	
			$\beta$ - phellandrene	Inc.	11142	
			Linalool	Inc.	6549	
17	<i>Cinnamomum zeylanium</i>	<i>Cannelle</i>	E-cinnamaldehyde	24.8 – 60.7	637511	61, 68
			Cinnamyl acetate	12 - 15,2	5282110	
			$\beta$ - caryophyllene	13	6429274	
			p- cimene	2.19	7463	
			Camphene	0.23 – 2.12	6616	
			Linalool	0.69 – 4.16	6549	
			Eugenol	14.78- 89.83	3314	

(INC\*) means « unknown »

**Appendix 6** Interaction energy of phytomolecules with the targeted nsps

N°	Phytomolecules	Binding energy (kcal/mol)				
		3CLpro	PLpro	RdRp	Helicase	2- OMTase
1	Copaborneol	-5.4	-5.7	-6.0	-5.9	-5.8
2	1,8 cineol	-4.2	-4.5	-4.7	-4.7	-4.9
3	Capsicodendrin	-8.0	-7.3	-7.9	-8.0	-8.1
4	Ishwarane	-5.4	-5.5	-6.0	-6.2	-6.3
5	Bicyclogermacrene	-5.2	-5.6	-5.4	-5.7	-5.8
6	Ugandensolide	-6.4	-6.9	-6.5	-7.8	-6.4
7	$\alpha$ -amorphene	-5.4	-5.8	-5.8	-5.6	-6.2
8	$\gamma$ -Curcumene	-5.4	-6.0	-4.7	-5.0	-6.1
9	Cinnamolide	-6.0	-6.1	-6.3	-6.6	-8.0
10	Viridiflorol	-5.8	-5.5	-5.8	-6.4	-6.2
11	Gingerdiol	-5.8	-5.8	-5.4	-5.5	-6.6
12	$\alpha$ -cadinol	-6.0	-5.7	-5.9	-6.0	-6.4
13	Tocotrienol	-6.8	-6.4	-6.0	-6.3	-7.2
14	(Z)-ajoene	-4.3	-4.4	-3.8	-4.4	-3.8
15	$\beta$ -elemene	-5.0	-5.4	-5.1	-5.6	-4.9
16	$\beta$ -caryophyllene	-5.2	-5.3	-5.5	-6.0	-5.2
17	(E)-Ajoene	-4.1	-4.0	-3.8	-4.4	-3.8
18	Cis Ocimene	-4.5	-5.1	-4.5	-4.9	-4.6
19	Geranyl tiglate	-5.6	-5.9	-4.6	-6.0	-5.1
20	Geranyl propanoate	-5.1	-5.7	-4.7	-5.3	-4.7
21	Methyl diacetoxo-6-gingerdiol	-6.1	-5.6	-5.0	-6.4	-5.0
22	Germacrene D	-5.4	-5.4	-5.1	-6.1	-5.1
23	Nerolidol	-5.5	-5.9	-4.7	-5.1	-5.2
24	Cinnamyl acetate	-5.2	-5.8	-4.9	-5.7	-4.7
25	Geranyl formate	-4.7	-5.1	-4.1	-5.4	-4.2
26	Trans-6- shogaol	-5.8	-5.8	-5.1	-6.3	-5.1
27	Isoalliin	-4.8	-4.8	-4.9	-5.3	-4.1
28	T-Muurolol	-5.8	-5.9	-5.8	-5.9	-5.0
29	Cadinene	-5.4	-5.4	-5.2	-5.7	-4.9
30	Nerol	-4.6	-5.2	-4.6	-4.9	-4.3
31	Geranial	-4.5	-5.0	-4.5	-5.0	-4.6
32	Geraniol	-4.7	-5.0	-4.3	-4.6	-4.4
33	E-cinnamaldehyde	-4.4	-4.9	-4.7	-4.9	-4.1
34	6,9-Guaiadiene	-5.2	-5.4	-5.6	-5.7	-5.4
35	Bicyclosesquiphellandrene	-5.2	-6.0	-5.5	-5.8	-5.4
36	$\Delta$ -3-Carene	-4.2	-5.0	-4.4	-4.8	-4.5
37	$\alpha$ -terpinenol	-4.9	-5.0	-4.8	-4.9	-4.7

38	$\beta$ - selinene	-5.5	-5.6	-5.4	-6.2	-5.1
39	Cinnamodial	-5.6	-5.6	-6.3	-6.9	-5.7
40	Pereniporin B	-6.0	-6.4	-6.2	-6.9	-6.0
41	Globulol	-5.6	-5.6	-5.5	-6.3	-5.4
42	Trans carveol	-5.0	-5.0	-4.9	-5.0	-4.6
43	Bornyl acetate	-5.3	-5.1	-5.1	-5.8	-4.8
44	Alliin	-4.7	-4.3	-4.6	-5.1	-4.2
45	Allicin	-4.6	-3.9	-3.5	-3.6	-3.3
46	Borneol	-4.3	-4.3	-5.0	-4.8	-4.3
47	Myrcene	-4.1	-4.8	-3.8	-4.2	-4.0
48	Zingerone	-5.4	-5.4	-4.9	-6.2	-4.8
49	Limonene	-4.4	-5.0	-4.6	-4.7	-4.5
50	Sabinene	-4.4	-4.4	-4.3	-4.6	-4.4
51	$\alpha$ - thujene	-4.4	-4.3	-4.4	-4.7	-4.3
52	$\alpha$ - terpineol	-4.8	-5.1	-4.8	-4.9	-4.8
53	Diallyl disulfide	-3.1	-3.5	-2.9	-3.0	-3.1
54	Diallyl trisulfide	-3.3	-3.7	-3.0	-3.3	-3.1
55	$\beta$ - pinene	-4.4	-4.4	-4.9	-4.6	-4.5
56	Isoterpinene	-4.9	-5.1	-4.5	-5.3	-4.6
57	Terpinen-4- ol	-4.8	-4.9	-4.8	-4.8	-4.8
58	$\beta$ - phellandrene	-4.8	-5.0	-4.7	-4.9	-4.7
59	Citronellol	-4.6	-4.9	-4.3	-4.6	-4.5
60	Methyl chavicol	-4.8	-4.9	-4.6	-5.3	-4.6
61	$\beta$ - terpineol	-4.7	-5.0	-4.7	-4.8	-4.8
62	Linalyl acetate	-4.5	-5.5	-4.8	-5.4	-4.6
63	Decanal	-3.9	-4.4	-3.6	-4.1	-3.3
64	Citronellyl formate	-4.6	-5.1	-4.3	-5.1	-4.4
65	p-cymene	-4.6	-5.0	-4.6	-4.9	-4.3
66	$\gamma$ -terpinene	-4.6	-5.0	-4.6	-4.8	-4.4
67	$\alpha$ - phellandrene	-4.5	-5.0	-4.4	-4.9	-4.6
68	Methyl isoeugenol	-4.8	-5.0	-4.9	-5.5	-4.5
69	Methyl eugenol	-4.7	-5.1	-4.6	-5.4	-4.5
70	Thymol	-4.7	-5.1	-4.9	-5.0	-5.0
71	Isomenthone	-4.1	-5.1	-4.7	-4.6	-4.4
72	$\alpha$ -pinene	-4.0	-4.5	-4.8	-4.6	-4.4
73	Camphene	-3.9	-4.4	-4.7	-4.7	-4.4
74	Linalool	-4.8	-5.2	-4.2	-4.5	-4.5
75	Eugenol	-4.8	-5.1	-4.8	-5.3	-4.6
76	2-camphanone	-4.4	-4.4	-4.7	-4.8	-4.3